agriculture

MDPI

Article

Vegetation Phenology Changes and Recovery after an Extreme Rainfall Event: A Case Study in Henan Province, China

Yinghao Lin [1,2], Xiaoyu Guo [1], Yang Liu [1], Liming Zhou [1], Yadi Wang [1,2], Qiang Ge [1,*] and Yuye Wang [1]

[1] Henan Key Laboratory of Big Data Analysis and Processing, School of Computer and Information Engineering, Henan University, Kaifeng 475001, China; linyh@henu.edu.cn (Y.L.); guoxy718@163.com (X.G.); sea@vip.henu.edu.cn (Y.L.); lmzhou@henu.edu.cn (L.Z.); yadiwang@henu.edu.cn (Y.W.); wangyuye@henu.edu.cn (Y.W.)

[2] Shenzhen Research Institute of Henan University, Shenzhen 518000, China

* Correspondence: gq@henu.edu.cn

Abstract: Extreme rainfall can severely affect all vegetation types, significantly impacting crop yield and quality. This study aimed to assess the response and recovery of vegetation phenology to an extreme rainfall event (with total weekly rainfall exceeding 500 mm in several cities) in Henan Province, China, in 2021. The analysis utilized multi-sourced data, including remote sensing reflectance, meteorological, and crop yield data. First, the Normalized Difference Vegetation Index (NDVI) time series was calculated from reflectance data on the Google Earth Engine (GEE) platform. Next, the 'phenofit' R language package was used to extract the phenology parameters—the start of the growing season (SOS) and the end of the growing season (EOS). Finally, the Statistical Package for the Social Sciences (SPSS, v.26.0.0.0) software was used for Duncan's analysis, and Matrix Laboratory (MATLAB, v.R2022b) software was used to analyze the effects of rainfall on land surface phenology (LSP) and crop yield. The results showed the following. (1) The extreme rainfall event's impact on phenology manifested directly as a delay in EOS in the year of the event. In 2021, the EOS of the second growing season was delayed by 4.97 days for cropland, 15.54 days for forest, 13.06 days for grassland, and 12.49 days for shrubland. (2) Resistance was weak in 2021, but recovery reached in most areas by 2022 and slowed in 2023. (3) In each year, SOS was predominantly negatively correlated with total rainfall in July (64% of cropland area in the first growing season, 53% of grassland area, and 71% of shrubland area). In contrast, the EOS was predominantly positively correlated with rainfall (51% and 54% area of cropland in the first and second growing season, respectively, and 76% of shrubland area); however, crop yields were mainly negatively correlated with rainfall (71% for corn, 60% for beans) and decreased during the year of the event, with negative correlation coefficients between rainfall and yield (−0.02 for corn, −0.25 for beans). This work highlights the sensitivity of crops to extreme rainfall and underscores the need for further research on their long-term recovery.

Keywords: crop yield; Duncan analysis; Google Earth Engine; NDVI; vegetative growth; phenological parameters; climate variability

Citation: Lin, Y.; Guo, X.; Liu, Y.; Zhou, L.; Wang, Y.; Ge, Q.; Wang, Y. Vegetation Phenology Changes and Recovery after an Extreme Rainfall Event: A Case Study in Henan Province, China. *Agriculture* **2024**, *14*, 1649. https://doi.org/10.3390/agriculture14091649

Academic Editor: Mohsin Tanveer

Received: 8 August 2024
Revised: 12 September 2024
Accepted: 18 September 2024
Published: 20 September 2024

1. Introduction

Vegetation phenology, the study of seasonal changes in plant communities, is crucial for understanding ecosystem functioning and strongly influences the carbon balance of ecosystems [1]. Phenological changes serve as primary cues for species to adjust to climate anomalies and such changes are sensitive to extreme climate events. However, the response mechanisms involved vary depending on the study area and vegetation types [2,3]. For instance, Shen et al. [4] found that alpine vegetation had the greatest temperature sensitivity (−3.3 °C/day) but the lowest rainfall sensitivity (−0.024 day/mm) for the start of the growing season (SOS), while steppe vegetation had the lowest temperature sensitivity (−1.9 °C/day) yet the greatest rainfall sensitivity (−0.108 day/mm). Piao et al. [5] demonstrated that extreme cold conditions have led to a delay in SOS and an advance at the

end of the growing season (EOS). Gong et al. [6] investigated the impacts of Hurricane Michael—it struck the U.S. Gulf of Mexico on 10 October 2018—on vegetation phenology in local subtropical longleaf pine forest sites, finding that this hurricane hastened post-storm fall senescence, leading to a 33-day advancement in EOS and 95-day reduction in the length of the growing season (LOS) at xeric sites. Liu et al. [7] identified a positive correlation between pre-season mean air temperature, total rainfall, and EOS by investigating vegetation phenology in China's temperate regions from 1982 to 2011. Most recently, Sun et al. [8] investigated how vegetation phenology responded to extreme temperature and rainfall events that differed in intensity on the Tibetan Plateau, from 2000 to 2018. Their work showed that high-intensity rainfall has advanced the SOS in about 54% of the region's area and delayed the EOS in 65% of it, that hot weather has advanced both the SOS and EOS in about 60% of the region, and that severe cold weather has delayed the SOS but advanced the EOS in 60% of the region.

Henan Province, located in the middle and lower reaches of the Yellow River Basin in east-central China, has a well-developed agricultural industry and a cropland area of about 81,500 km^2, ranking it second among the country's provincial cropland areas. Several scholars have studied the vegetation phenology in this province. Zhang et al. [9] quantified the effects of temperature, rainfall, solar radiation, and wind on maize phenology, from 1971 to 2020, by using a comprehensive climate suitability model. This revealed temperature and rainfall as the main climatic factors affecting yield variability, while low sunshine and high winds could adversely impact crop yield to some extent. Liu et al. [10] quantitatively analyzed the spatiotemporal changes in maize phenology and its sensitivity to changes in major climatic factors, from 1981 to 2009, by using a climate tendency rate and sensitivity analysis. Their findings uncovered a rate of change of –0.01 day/a to –0.17 day/a for the seedling-to-maturity phase of maize, with the LOS changing (increasing) at a rate of 0.04 day/a. Yet far fewer studies have addressed the mechanisms by which extreme climatic events alter phenology, whose research is imperative [3,11].

On or around 20 July 2021, Henan Province experienced a rare and large-scale extreme rainfall disaster, known as the "7.20" event. According to the China Meteorological Administration, the heavy rainfall was caused chiefly by an immense volume of water vapor brought by Typhoon In-Fa. The terrain exacerbated the risk situation, leading to huge amounts of rainfall falling on windward slopes. Waterlogged crops incurred oxygen deficiency in their roots, growth inhibition, dieback, and collapse, as well as greater susceptibility to pests and diseases. Altogether, this caused severe damage to crops such as corn and soybeans, culminating in stark declines in their yield and quality, serious economic losses for farmers, and extensive damage to the province's agroecosystems [12].

Remote sensing technology, due to its capacity for large-scale observations at relatively low costs, has become an essential tool in disaster and risk monitoring [13,14]. The Normalized Difference Vegetation Index (NDVI), derived from the Moderate Resolution Imaging Spectroradiometer (MODIS), has been widely used to invert land surface phenology (LSP) [15]. Using the Google Earth Engine (GEE) platform, Pan et al. [16] analyzed Landsat 7/8 and Sentinel 2A/B surface reflectance data NDVI to extract the phenological characteristics of different vegetation types to delineate the planted area of winter crops in their study area. Agriculture is the economic backbone of Henan Province, and flooding there caused by extreme rainfall is a prominent threat to its crop yields. This paper takes the extreme rainfall event in July 2021 as an example and Henan Province as the study area. The NDVI time series was first generated using surface reflectance data from 2018–2023. Next, the SOS and EOS of these six years were extracted and the changes in phenology and recovery after the event were calculated. Finally, corn and bean yield data along with meteorological data were combined to examine correlations between rainfall and phenology or yield. The results can provide valuable insights for improving ecological protection, management, ecosystem services, and disaster prevention and mitigation policy-making in Henan Province.

2. Materials and Methods

2.1. Study Area

Henan Province spans 31°23′ N to 36°22′ N in latitude and 110°21′ E to 116°39′ E in longitude, encompassing 167,000 km^2. Henan has a continental monsoon climate, transitioning from a warm temperate zone in its north to a subtropical zone in its south [17]. The east-central region of Henan is experiencing an increasing frequency of extreme rainfall events. Over the past 50 years, rainfall has gradually declined from south to north, resulting in marked differences between the regions, with an average annual rainfall of 735.94 mm [18]. Rainfall is largely concentrated in June, July, and August, which together account for 60% to 70% of the annual total. Henan is one of the political, economic, and cultural centers of China. By the end of 2023, its permanent population reached 98.15 million, ranking it third in total population at the provincial level [19].

Henan is also a typical Chinese province with multiple growing seasons per calendar year. The single-growing season is prevalent in the western and southern mountainous regions of Henan, with forests and natural grasslands predominating in the west, and single-season rice fields dominant in the south. The double-growing season region is mainly located in the eastern plains of Henan, which is prime agricultural land, with the first growing season used to cultivate winter wheat and the second for corn, peanuts, and soybeans. The triple-growing-season region is less common, being sporadically distributed in Henan's northern part in which vegetables are mainly cultivated [20]. As shown in Figure 1, the vegetation types in the study areas where the total rainfall exceeded 500 mm in the week before and after the '7.20' extreme rainfall event (hereon referred to as the extreme rainfall zone) consist mostly of cropland, followed by shrubland, with a few patches of forest and grassland. Representative sample points were labeled representative sample points for four different vegetation types: cropland, shrubland, forest, and grassland (in both extreme and non-extreme rainfall zones).

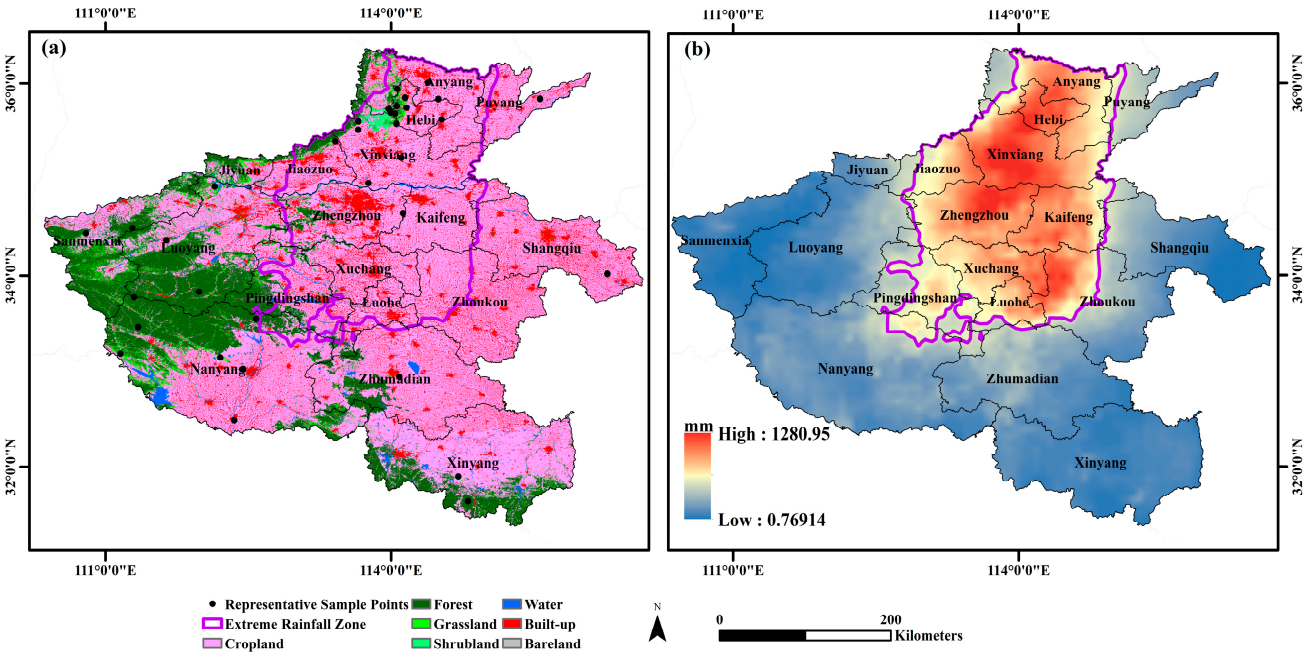

Figure 1. (**a**) Map of the study area, Henan Province (China), and the distribution of its land cover types. (**b**) Cumulative rainfall from 17 July to 23 July 2021. The irregular purple line-demarcated zone is where the cumulative rainfall exceeded 500 mm, with its cities delineated by gray lines.

2.2. Data

This study used the 2020 version of the 30-m global surface coverage data GlobeLand30, published by the National Geomatics Center of China [21]. They were produced by the Ministry of Natural Resources of China and donated to the United Nations on 15 September 2020, the 75th anniversary of the latter's founding. The three-season vegetable growing areas mentioned in this study are subsumed under the cropland category of this dataset.

When using the Maximum Value Composite approach, the 8-d or 16-d resolution MODIS vegetation index products may lose values for important phenological transition dates [22,23]. Further, NDVI is more sensitive than other metrics in detecting differences in LSP parameters [24]. So, based on the GEE platform [25] and using the atmospherically corrected "MODIS/Terra Surface Reflectance Daily L2G Global 1 km and 500 m SIN Grid v061" (MOD09GA) [26] product, NDVI time series with a temporal resolution of 3 days and a spatial resolution of 500 m for the 2018–2023 period were batch computed [27]:

$$\mathrm{NDVI} = \frac{\mathrm{NIR} - \mathrm{RED}}{\mathrm{NIR} + \mathrm{RED}} \quad (1)$$

In the above equation, NIR is the reflectance value for the near-infrared band (841–876 nm), and RED is the reflectance value for the red band (620–670 nm). The value of NDVI can range from −1 to 1, with larger positive values representing greater vegetation greenness, and smaller positive values representing less vegetation greenness; negative values represent non-vegetation types, such as clouds, water, and snow as ground cover [28,29].

The annual production (weight) data and planted area data of corn and bean in the study area were obtained from the statistical yearbook compiled by the Henan Provincial Bureau of Statistics [30]. Yield in this study was defined as weight divided by planted area, in units of 'tons ha^{-1}'.

The Climate Prediction Center Morphing Technique (CMORPH), developed by the National Oceanic and Atmospheric Administration's Climate Prediction Centre of the United States of America (NOAA/CPC, [31]), was used to visualize rainfall and associated data calculations in this study. This dataset has a temporal resolution of 30 min and a spatial resolution of 8 km. The calculation of total rainfall was performed in MATLAB (v.R2022b) software, using the 'cmorph' band of the rainfall NetCDF file, with a data matrix of 2 × number of rows × number of columns, where 2 corresponds to the two values of rainfall for one hour. The total rainfall was calculated by adding up the two layers, with the spatial resolution resampled to the same as that of the NDVI data.

2.3. Methods

The GEE platform and a personal desktop computer were used to conduct this study. As illustrated in Figure 2, NDVI time series were first calculated from reflectance data in the GEE platform. Next, the R environment (R v.4.3.3 and R Studio v.2023.06.2+561, [32]) was used for the phenology parameters' extraction, with SPSS (v.26.0.0.0) software used for Duncan's analysis and MATLAB (v.R2022b) software to analyze the effects of total rainfall upon NDVI and LSP [33,34].

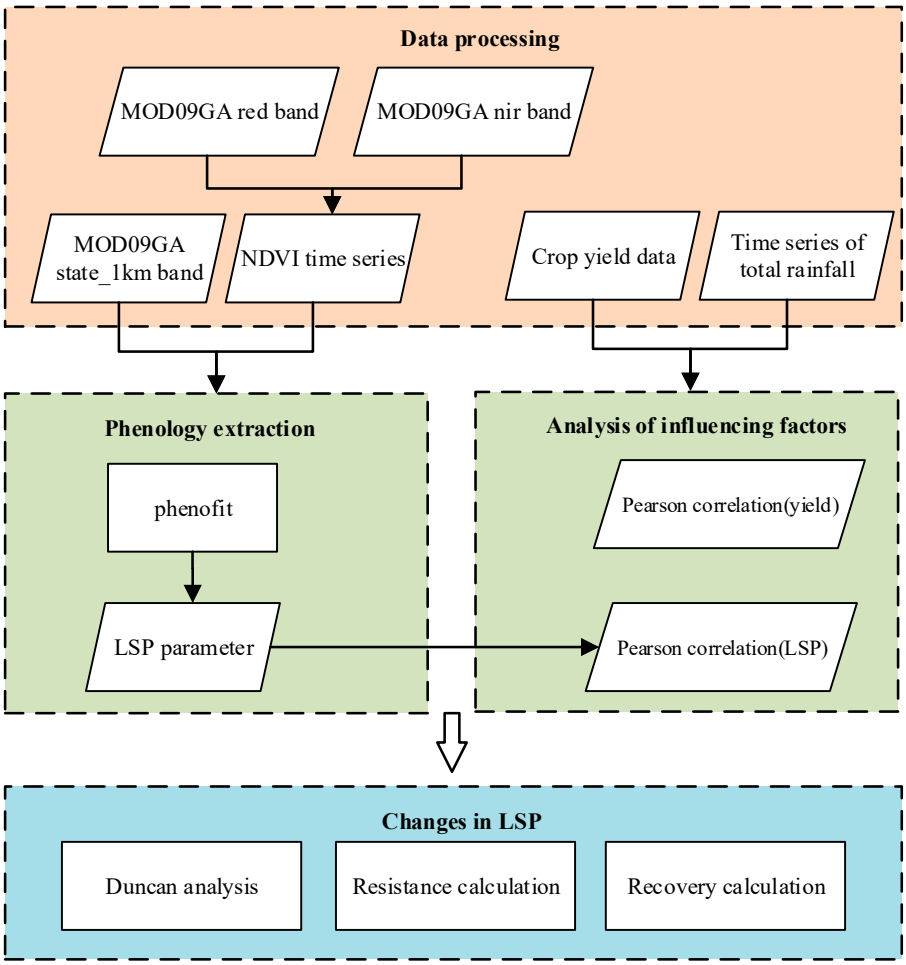

Figure 2. The flowchart of this vegetation phenology study.

2.3.1. Extraction of Phenology Indicators

To extract the phenology indicators, the 'phenofit' package of Kong et al. [20] was used because it can categorize the number of growing seasons per pixel and is suitable for phenology extraction in multi-season crop areas. The 'qc_StateQA' function was used to initialize the weights based on the quality assessment band "state_1km" of MOD09GA data; pixel weights were set to 1 (no cloud, snow, aerosol), 0.2 (cloud, snow, aerosol), and 0.5 (all other cases) based on a pixel's value in this band.

The 'check_input' function was utilized to discard any spikes and missing values for the time-series NDVI. The boundary ylu was defined as the upper and lower quartiles of the data, and those point values outside the boundary were designated the lower ylu boundary, with 0.02 assigned as their point weights. To delineate the number of growing seasons, a coarse fit was performed using the 'wSG' function with the parameter frame set to 48. A fine fit was then performed using the 'Beck' function to capture the rapid changes in vegetation during each growing season. The 'wTSM weight update' function was applied to adjust the weight values during the fitting process. Finally, the 'TRS' thresholding method was employed to extract the phenology parameters.

2.3.2. Resistance and Recovery Rates of Vegetation and Rainfall Recovery Rates

Two evaluation metrics of ecosystem resilience were used to assess the resistance, R_t, and recovery, R_c, of forest, grassland, and shrubland vegetation to the extreme rainfall event. For crops, given that these are annual plants, the recovery rate R_{cp} of rainfall in 2022

and 2023 was considered to measure the stability of the environment of such plots. The equations for each are as follows [35–37]:

$$R_t = \frac{NDVI_1}{NDVI_0} \tag{2}$$

$$R_c = \frac{NDVI_i - NDVI_1}{NDVI_0 - NDVI_1} \tag{3}$$

$$R_{cp} = \frac{p_i - p_1}{p_0 - p_1} \tag{4}$$

where, $NDVI_0$ is the NDVI before the extreme rainfall event (2020); $NDVI_1$ is the NDVI in the year of the extreme rainfall event (2021); and $NDVI_i$ is the NDVI in each year after the event (2022, 2023). The p_0 is the rainfall before the extreme rainfall event (2020); p_1 is the rainfall in the year of the extreme rainfall event (2021); and p_i is the rainfall in each year after the event (2022, 2023). Larger values indicate greater resistance. Recovery can then be categorized into six ratings, as shown in Table 1, based on the R_c and R_{cp} values obtained [38].

Table 1. Recovery rating scores and their quantification and qualification.

Rating	Range of Recovery	Recovery
1	<0	Poor
2	0–0.25	Relatively poor
3	0.25–0.5	Average
4	0.5–0.75	Relatively good
5	0.75–1.0	Good
6	>1	Fully

2.3.3. Data Analysis

Many research methods have been used to study changes in vegetation phenology and correlations between variables [39,40]. The present study relied on three methods:

(1) For each vegetation type, a one-way analysis of variance (ANOVA) was used to determine the temporal effect of extreme rainfall on each phenological parameter. That is, whether the SOS differed among three subperiods: before and during the extreme (2018~2021), one year (2022) after extreme rainfall, and two years (2023) after extreme rainfall; and whether EOS differed among four subperiods: before the extreme rainfall (2018~2020), the year of extreme rainfall (2021), the year after extreme rainfall (2022), and two years after extreme rainfall (2023). Before performing the ANOVA, tests for normality and homogeneity of variances were conducted to ensure the validity of the analysis. Then, after each ANOVA, Duncan's multiple range test—which can provide careful analysis of between-group differences—was used for the pairwise statistical comparisons of the mean values of each phenological parameter between the treatment groups (i.e., subperiods).

(2) The spatial correlation of rainfall data from 2018 to 2023 with SOS or EOS, as well as that from 2018 to 2022 with crop yield, was analyzed using Pearson's correlation coefficient, which was calculated in MATLAB (v.R2022b) software using Equation (4) [39]:

$$r = \frac{\sum_{i=1}^{n}(p_i - \overline{p})(x_i - \overline{x})}{\sqrt{\sum_{i=1}^{n}(p_i - \overline{p})^2 \sum_{i=1}^{n}(x_i - \overline{x})^2}} \tag{5}$$

where p_i is the total rainfall in July of the year i; x_i is the phenological parameter (SOS or EOS) or yield data of year i; and $\overline{p}$ and $\overline{x}$ are the average values of rainfall and phenology or the mean yield of year n, respectively. The value of r ranges from -1 to

1, and the larger the absolute value of r is, the larger the effect of rainfall on phenology or yield, and vice versa.

(3) The correlation between rainfall and crop yield for a given year was calculated using the Pearson correlation coefficient in SPSS (v.26.0.0.0) software [41], as per Equation (5):

$$\rho_{m,n} = \frac{cov(m,n)}{\sigma_m \sigma_n} \quad (6)$$

In the above equation, m is the total rainfall in July annually, and n is the annual corn or bean yield.

3. Results

3.1. Changes in Phenology after Extreme Rainfall

The changes in the NDVI of representative pixels of each vegetation type from 2018 to 2023 are shown in Figure 3, since shrubland pixels are all distributed in the extreme rainfall zone, there is no non-extreme rainfall zone data for shrubland. Irrespective of type, the vegetation index in the extreme rainfall zone decreased after the extreme rainfall event of "7.20" in 2021. Furthermore, for both cropland and grassland, their curves are lower in the extreme rainfall zone than in the non-extreme rainfall zone.

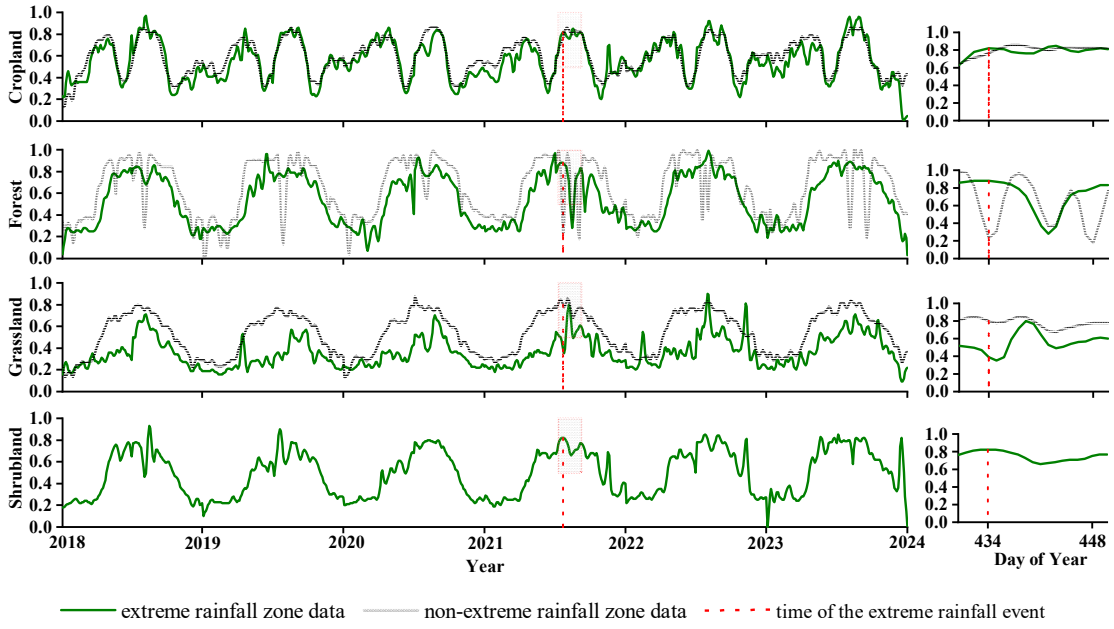

Figure 3. Trends in the NDVI of each vegetation type, from 2018 to 2023. Green curves show representative sample point values in the extreme rainfall zone while gray curves show those in non-extreme rainfall zone; the vertically dashed red lines and red rectangles mark the occurrence of the extreme rainfall event in 2021 in Henan Province (China).

These trends in NDVI highlight the immediate impact of extreme rainfall events on vegetation health. To further quantify this effect and assess the impact on the phenology of each vegetation type, ANOVA analyses were conducted, with the results summarized in Table 2.

The mean values of SOS (SOS1) for the first growing season of cropland were significantly different from those for pre-extreme rainfall, advancing by 2.33 days in 2022, but delayed significantly in 2023. Mean values for EOS (EOS1) were significantly delayed by 3.04 days in 2022 and by another 0.37 days in 2023. Mean values of SOS for the second growing season (SOS2) differed significantly from those for pre-extreme rainfall with a delay of 1.4 days in 2022 and another significant delay in 2023. Although the mean EOS

(EOS2) was significantly delayed by 4.97 days after extreme rainfall in 2021, it arrived significantly earlier in 2022 but then significantly later in 2023.

Table 2. Results of the variance analysis (ANOVA) testing the temporal impact of an extreme rainfall event on LSP parameters. Different letters indicate significant differences within each column subset at the $p < 0.05$ level, with a to d corresponding to increasing mean values.

Vegetation Type	LSP	*p* Value	Years	Mean
Cropland	SOS1 *	0	2018–2021	32.28 (b)
			2022	29.95 (a)
			2023	42.39 (c)
	EOS1 *	0.006	2018–2021	144.40 (a)
			2022	147.44 (b)
			2023	147.81 (c)
	SOS2 *	0	2018–2021	180.82 (a)
			2022	182.22 (c)
			2023	181.62 (b)
	EOS2 *	0	2018–2020	272.73 (a)
			2021	277.70 (c)
			2022	275.47 (b)
			2023	283.00 (d)
Forest	SOS	0	2018–2021	85.58 (a)
			2022	85.91 (b)
			2023	88.09 (c)
	EOS	0	2018–2020	318.02 (a)
			2021	333.56 (d)
			2022	321.80 (b)
			2023	325.63 (c)
Grassland	SOS	0.101	2018–2021	86.60 (a)
			2022	86.36 (a)
			2023	88.34 (b)
	EOS	0.954	2018–2020	315.60 (a)
			2021	328.66 (c)
			2022	324.09 (b)
			2023	323.94 (b)
Shrubland	SOS	0.063	2018–2021	99.46 (b)
			2022	96.86 (a)
			2023	100.14 (c)
	EOS	0.998	2018–2020	313.90 (a)
			2021	326.39 (c)
			2022	316.61 (b)
			2023	326.28 (c)

* SOS1 and EOS1 represent the phenology parameters for the first growing season, whereas SOS2 and EOS2 correspond to the phenology parameters for the second growing season.

For forest vegetation, the mean SOS was significantly delayed by 0.33 days in 2022, the year after the extreme rainfall event, in comparison to the pre-extreme rainfall mean, and then significantly delayed by 2.18 days in 2023. The mean EOS in 2021 was significantly different from the pre-extreme rainfall mean, with a delay of 15.54 days on average; however, in 2022, one year after the event, the EOS had significantly advanced by 11.76 days. Nevertheless, in 2023, the EOS mean value was again significantly delayed vis-à-vis the previous year, but still earlier than 2021, which may be attributed to the greater total rainfall in 2023.

Grassland vegetation exhibited a mean SOS in 2022 that was comparable to pre-extreme rainfall conditions, with an average advance of 0.24 days. However, there was a significant difference between the grassland's mean SOS in 2023 and that before the event,

corresponding to a delay of 1.98 days. Compared with mean values for 2018 to 2020, the mean EOS in 2021 was significantly delayed by 13.06 days, and in 2022 it was significantly advanced by 4.57 days, albeit not returning to pre-extreme rainfall levels. No significant differences were found between 2023 and 2022.

For shrubland vegetation, the mean SOS in 2022 differed significantly from that for pre-extreme rainfall, coming 2.6 days earlier on average, and then delayed significantly in 2023. The mean EOS was significantly different between pre-extreme rainfall versus after the event in 2021, being delayed by 12.49 days on average. Although the EOS did come significantly earlier in 2022, it did not recover to pre-rainstorm levels, and it was significantly delayed again in 2023.

3.2. Spatiotemporal Patterns of Resistance and Recovery

The results for the resistance (R_t) and recovery (R_c) of forest, grassland, and shrubland vegetation after the extreme rainfall event are illustrated in Figure 4. The overall resistance of the forest (R_tNDVImean = 0.91) indicated a reduction in its NDVI across the study area. In 2022, the forest recovery was not ideal (R_cNDVImean = −1.99); however, good forest recovery occurred in 2023 (R_cNDVImean = 0.89). For grassland, the overall resistance (R_tNDVImean = 0.90) revealed a decrease in NDVI. The NDVI did not recover in 2022 (R_cNDVImean = −1.65), but it did recover well in 2023 (R_cNDVImean = 0.99). Shrubland resistance also indicated a decrease in NDVI (R_tNDVImean = 0.88), with no recovery of NDVI in 2022 (R_cNDVImean = −1.21) followed by a good recovery in 2023 (R_cNDVImean = 0.77).

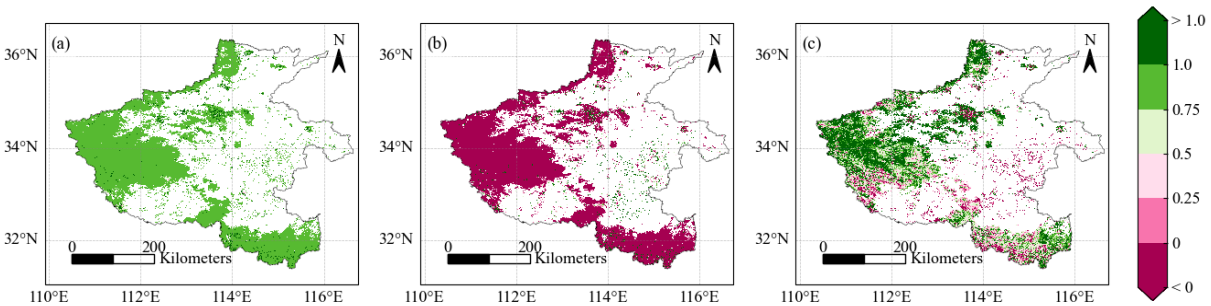

Figure 4. (**a**) Spatial distribution of resistance values of vegetation after the extreme rainfall event in 2021, in Henan Province, China. In (**b**,**c**) are the patterns of vegetation recovery in 2022 and 2023, respectively.

The mean values for the resistance and recovery of forest, grassland, and shrubland vegetation in the extreme rainfall zone are detailed in Table 3, indicating significant differences in recovery among the vegetation types. The potential reasons for these differences in sensitivity are discussed in Section 4.2.

Table 3. Mean resistance and recovery of forest, grassland, and shrubland vegetation in the extreme rainfall zone.

Vegetation Type	Resistance	Recovery in 2022	Recovery in 2023
Forest	0.90	−1.60	1.06
Grassland	0.92	−1.28	1.26
Shrubland	0.88	−1.21	0.77

Results for the recovery (R_{cp}) of rainfall in the distribution area of cropland after the extreme rainfall event are shown in Figure 5, revealing a moderate recovery in 2022 (R_{cp}mean = 0.59) and good recovery in 2023 (R_{cp}mean = 0.77) compared to the period before the extreme event.

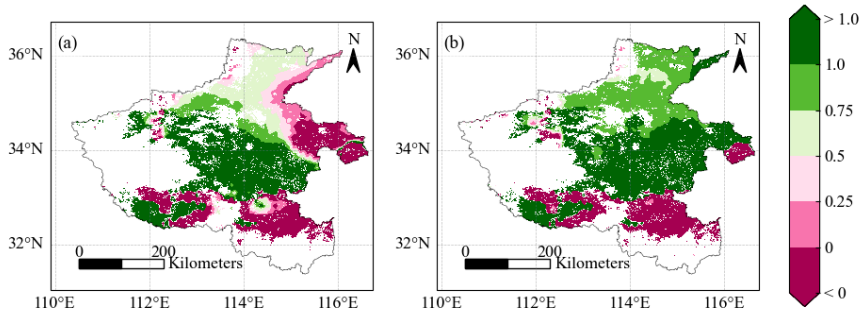

Figure 5. The patterns of rainfall recovery in (**a**) 2022 and (**b**) 2023, respectively.

3.3. Correlation between Rainfall and LSP

The spatial distribution of Pearson's correlation coefficients between cropland phenology and rainfall is shown in Figure 6. The proportion of pixels with a negative correlation between the SOS for cropland vegetation in the first growing season and the total rainfall in July was 64%, i.e., the SOS happened earlier as rainfall increased. However, 51% of the pixels featured a positive correlation between the EOS and the total rainfall in July, i.e., the EOS was delayed by more rainfall. In the second growing season, 53% and 54% of the pixels were, respectively, distinguished by positive correlations of SOS and EOS with total rainfall in July. Taken together, these results were consistent with the trends in phenology changes of cropland vegetation (top of Table 2).

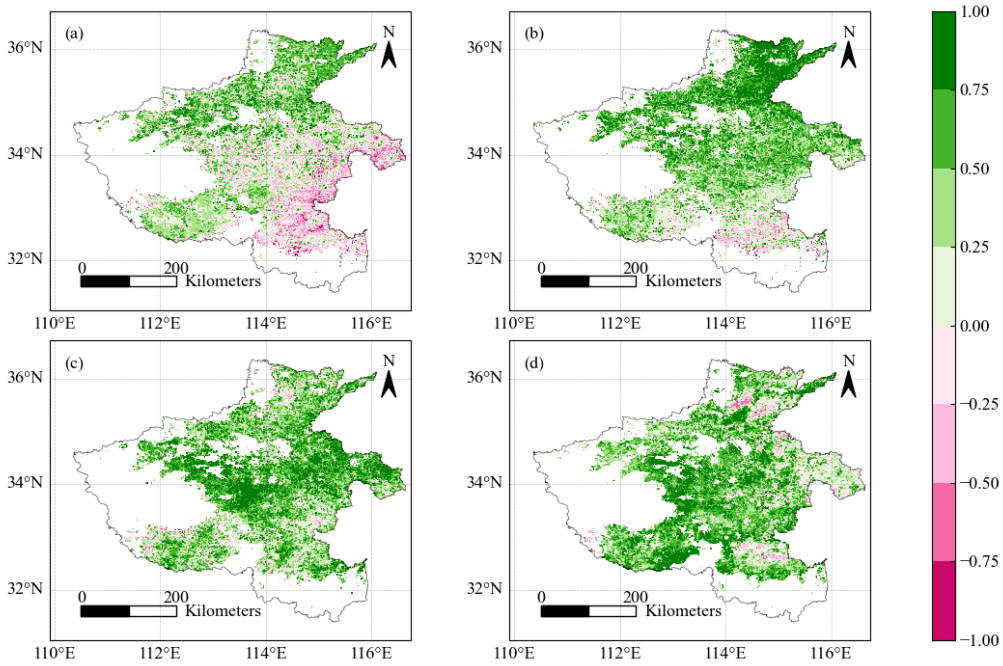

Figure 6. Spatial distribution of Pearson's *r* coefficient values in cropland: (**a**–**d**) are the correlations of SOS1, EOS1, SOS2, and EOS2 with rainfall, respectively.

The spatial distribution of Pearson's correlation coefficients between forest phenology and rainfall is shown in Figure 7. The analysis indicates that 39% of the pixels showed a negative correlation between the SOS of forest vegetation and total rainfall in July, whereas the proportion of pixels with a positive correlation was noticeably higher, at 59%. The proportion of pixels with a negative correlation between the EOS in July and total rainfall reached 55%, exceeding those with a positive correlation (43%).

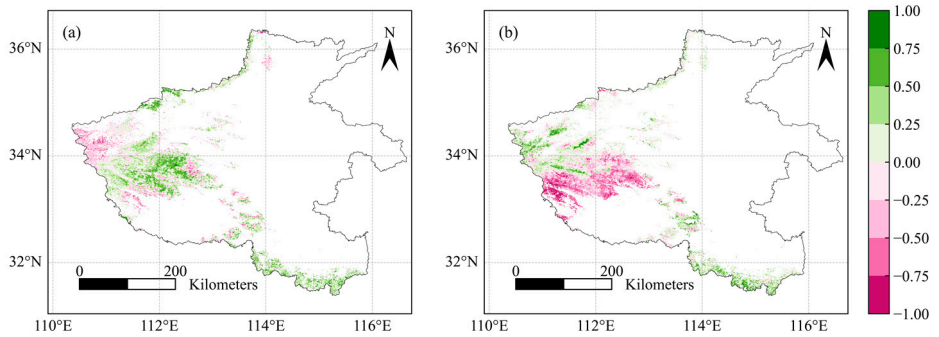

Figure 7. Spatial distribution of Pearson's *r* coefficient values for the forest (**a**) SOS and (**b**) EOS correlations with rainfall, in Henan Province, China.

The spatial distribution of Pearson's correlation coefficients between grassland phenology and rainfall is shown in Figure 8. Overall, 53% of the pixels had a negative correlation between the SOS of grassland vegetation and total rainfall in July, this is higher than those with a positive correlation (43%). The proportion of pixels with a negative correlation between the EOS and total rainfall in July reached 49%, only slightly higher than those with a positive correlation (47%).

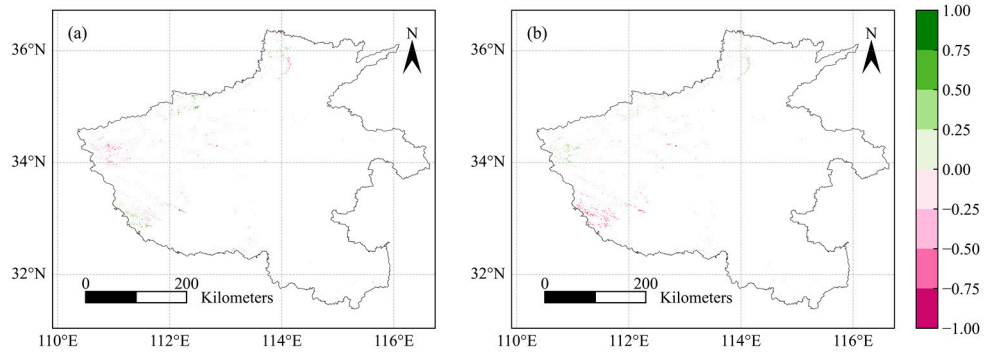

Figure 8. Spatial distribution of Pearson's *r* coefficient values for the grassland (**a**) SOS and (**b**) EOS correlations with rainfall, in Henan Province, China.

The spatial distribution of Pearson's correlation coefficients between shrubland phenology and rainfall is shown in Figure 9. The proportion of pixels with a negative correlation between the SOS of shrubland vegetation and total rainfall in July reached 71%, whereas the proportion of pixels with a positive correlation was much lower, at 26%. Conversely, 22% of the pixels showed a negative correlation between the EOS and total rainfall in July, with 76% of pixels being positively correlated.

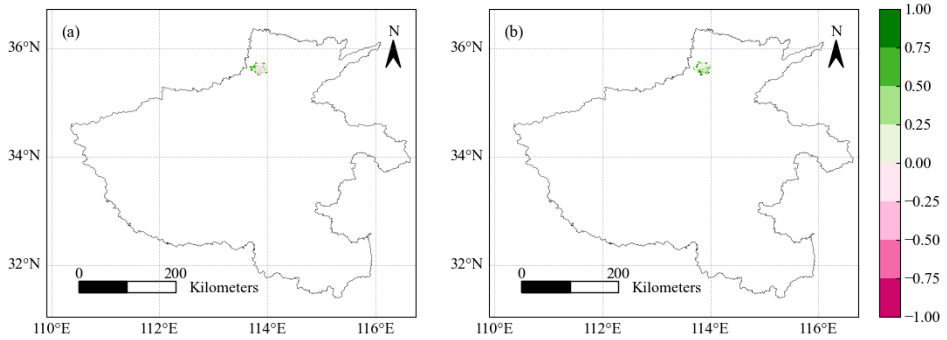

Figure 9. Spatial distribution of Pearson's *r* coefficient values for the shrubland (**a**) SOS and (**b**) EOS correlations with rainfall, in Henan Province, China.

3.4. Relationship between Rainfall and Crop Yield

The spatial distribution of Pearson's correlation coefficients for corn and bean yields vis-à-vis the 2018–2022 July rainfall is shown in Figure 10. Across the cropland region, 71% of the pixels showed a negative correlation between corn yield and rainfall, while the proportion of pixels that had a negative correlation between bean yield and rainfall was even higher, at 60%. These results indicated an increase in rainfall was associated with a decrease in yield.

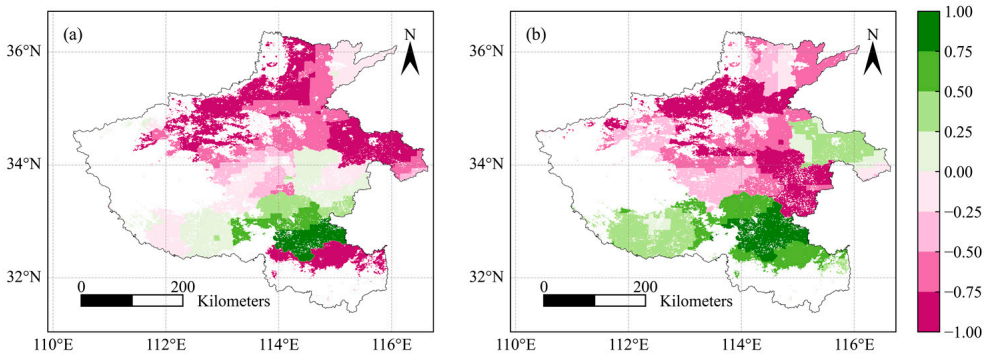

Figure 10. Spatial distribution of Pearson's *r* coefficients for the (**a**) corn yield and (**b**) bean yield correlations with rainfall, in Henan Province, China.

In the extreme rainfall zone, about 90% of the regions displayed a negative correlation between corn yield and rainfall, as shown in Table 4. Though not as pronounced, 98% of the regions also featured a negative correlation between bean yield and rainfall, and 10% of the pixels had a significant negative correlation.

Table 4. Percentage of correlation coefficients between crop yield and rainfall. Significant positive correlation: $r > 0$, $p < 0.05$. Significant negative correlation: $r < 0$, $p < 0.05$.

Crop	Correlation	Proportion
Corn	Positive correlation	9.9%
	Negative correlation	90.1%
	Significant positive correlation	0%
	Significant negative correlation	3.8%
Bean	Positive correlation	1.3%
	Negative correlation	98.4%
	Significant positive correlation	0%
	Significant negative correlation	10.0%

The correlation coefficients between rainfall and crop yield in a given year are detailed in Table 5 and were negative for both in 2021, indicating that the increase in rainfall led to decreased yields.

Table 5. Pearson correlations between crop yield and rainfall within each year.

Year	Corn Yield	Bean Yield
2018	0.09	0.25
2019	0.11	0.07
2020	−0.08	−0.52
2021	−0.02	−0.25
2022	0.49	0.56

4. Discussion

4.1. Changes in Rainfall by City

The average rainfall in July for each city from 2018 to 2023 is shown in Figure 11. Specifically, in 2021, the average rainfall exceeded 500 mm everywhere except Luoyang City, Sanmenxia City, and Jiyuan City, while rainfall was lowest in Sanmenxia City, which could explain why crop yield there did not decrease in 2021. In 2018 and 2019, the years preceding the heavy rainfall event of this study, the average July rainfall in each city did not exceed 400 mm. In 2020, under the influence of the north-south oscillation of the main rain belt in the Huaihe River Basin, six cities in southeastern Henan (Luohe, Nanyang, Shangqiu, Xinyang, Zhoukou, Zhumadian) received heavy rainfall, with rainfall exceeding 500 mm from 17–19 July [42]. In 2022, the year right after that (2021) of the heavy rainfall event, seven more cities (Kaifeng, Anyang, Hebi, Xinxiang, Puyang, Shangqiu, Zhumadian) received more than 500 mm of rainfall in July [21,43]. For example, the average rainfall in Hebi in July 2023 was nearly 1.8 times that for the same period over many years before [44], reaching 516 mm, while rainfall in the rest of Henan's affected cities returned to normal levels in that year.

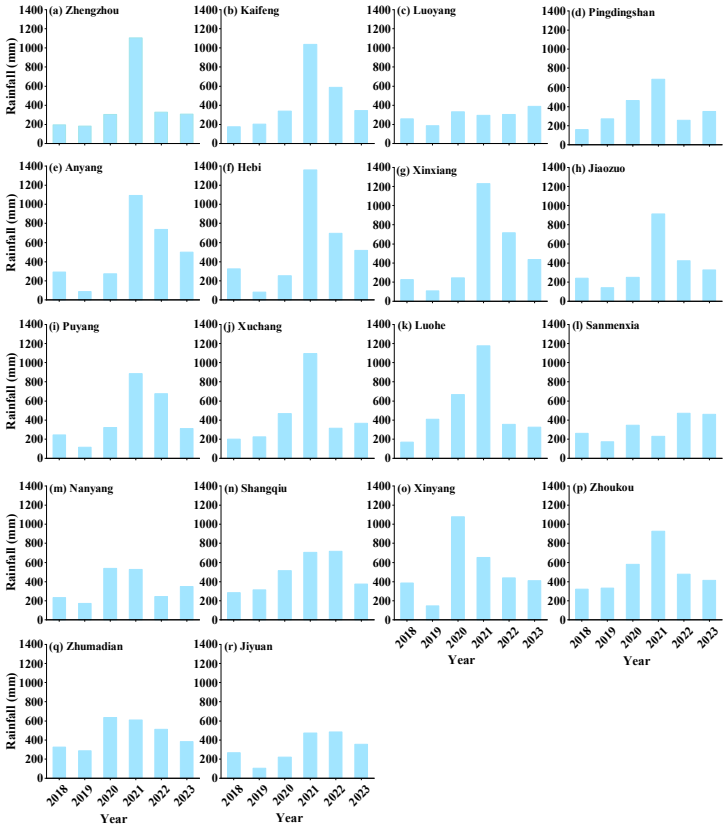

Figure 11. The average rainfall per city in July each year from 2018 to 2023.

4.2. Effects of Extreme Rainfall on Vegetation Phenology

Surprisingly few studies have investigated the response of vegetation phenology to extreme rainfall events. In this case study, MODIS reflectance data were used to calculate vegetation indices from which vegetation phenology parameters were derived. Specifically, this study explored changes in the phenology, resistance, and recovery of vegetation types after an extreme rainfall event and analyzed the factors affecting phenology in combination with climate data. The results indicate that, after the event, the temporal vegetation index curves of various vegetation types in the extreme rainfall area display a decrease, which can be explained by the low NDVI values of pixels caused by vegetation being submerged by flooding. The decrease in forests and shrubs is likely due to changes caused by plant

lodging and soil moisture saturation. Further, vegetation's resistance is weaker and the EOS is delayed. The phenological response strategy is affected by rainfall, and the recovery of vegetation differs between different municipalities 1 and 2 years after the event. This study found compelling evidence that the effect of extreme rainfall on the EOS in the same year of the event was mainly a postponement effect.

After the extreme rainfall event in 2021, generally, the SOS occurred earlier and the EOS was delayed. Furthermore, by 2023, vegetation conditions had not yet recovered to their pre-extreme rainfall levels, for which work by Hogan et al. [45] provides a valuable perspective on this phenomenon, pointing out that biodiversity and resilience together influence the recovery time of ecosystems.

Given that the extreme rainfall event occurred in July 2021, the correlation between vegetation phenology and total rainfall in July for each year was further explored. This set of results revealed that rainfall tends to be negatively related to the SOS and positively related to the EOS. This pattern is consistent with the findings of some scholars [8,46,47], yet it contradicts those of other studies [5,40,48,49]. This can be explained by different factors such as drought, fire, hurricanes, extreme cold, soil erosion, and anthropogenic disturbances (e.g., land use and land cover changes). For example, hurricanes can cause sudden loss of foliage and a rapid decline in the leaf area index of the plant community, so that the end of the growing season comes earlier for that vegetation [6,50]. There is also substantial heterogeneity in the interactions between extreme climatic events and different vegetation types [47,51,52]. The influence of climate on phenology is now undeniable. Huang et al. [53] demonstrated that the relative contribution of flooding to SOS2 was 80.1%. Work by Zhang et al. [54] showed that cumulative rainfall reached a certain threshold to stimulate vegetation greening, with a lag in vegetation dormancy of up to 84 days. Using multiple models, Zscheischler et al.'s [55] simulation results enable them to elucidate how ecosystem productivity is increased by extreme rainfall, which enhances the carbon sequestration capacity of terrestrial ecosystems.

4.3. Effects of Extreme Rainfall on Crop Yields

Henan is an important grain-producing province. This study's investigation of the rate of recovery of rainfall in its cropland distribution areas suggests that rainfall is recovering to pre-extreme-event levels on a yearly basis. The research on yield changes in the province shows that, in 2021, the total annual crop yields of all cities were lower than their prior mean, except for bean yields in Nanyang, Shangqiu, Xinyang and Zhumadian, which remained stable. Both corn and bean yields in 2022 rose in comparison to 2021, except for a drop in bean yield in Luoyang City, Pingdingshan, Nanyang, Shangqiu, and Zhumadian City, as shown in Table 6. However, the 2022 yields in most regions remain low compared to their 2018–2020 yields on average. According to the crop planted areas in each city, as detailed in Table 7, the planted areas in Zhengzhou, Pingdingshan, Anyang, Hebi, Xinxiang, Jiaozuo, Shangqiu, and Jiyuan cities did not decrease in 2021 compared to the average of the previous three years, but their grain yields decreased, indicating a generally negative impact of rainfall on crop yields. This phenomenon is consistent with the findings of Liu et al. [56], who pointed out that the physical damage caused by extreme rainfall events during the critical growth period of crops, accompanied by root hypoxia caused by oversaturated soils, can significantly affect the growth and development of crops, culminating in reduced yields. In contrast, the lower rainfall Sanmenxia and Luoyang cities still had lower crop yields, which correlated with the reduction in the planted areas of crops in those two cities.

The correlation analysis between yield and rainfall for 2018–2022 revealed that an increase in rainfall usually leads to a decrease in yield. This is similar to the findings of previous studies; for example, when Pantaleoni et al. [57] examined the impact of an extreme rainfall event on crop yields in Indiana in 2003, soybean yields were significantly lower after the event. The study also showed that although yields recovered in individual areas in some years, overall, the long-term effects of extreme rainfall events on cropland vegeta-

tion remained significant. Taken together, this emphasizes the importance of considering extreme weather events in agricultural management and disaster prevention.

Table 6. Annual crop yield of various cities in Henan Province, China.

Cities	Mean Yield * (tons ha^{-1})		Yield in 2021 (tons ha^{-1})		Yield in 2022 (tons ha^{-1})	
	Corn	Beans	Corn	Beans	Corn	Beans
Zhengzhou	4.94	1.90	4.48	1.67	4.81	1.81
Kaifeng	5.37	2.05	4.97	1.94	5.34	2.04
Luoyang	5.29	2.32	4.60	2.10	4.83	1.99
Pingdingshan	5.08	2.78	4.82	2.31	4.82	2.25
Anyang	6.67	2.39	4.70	2.05	6.36	2.54
Hebi	7.23	2.35	2.54	1.16	7.19	2.17
Xinxiang	6.22	3.17	4.55	1.88	5.96	2.78
Jiaozuo	7.33	3.05	5.40	2.11	7.09	2.74
Puyang	6.72	2.85	6.27	2.37	7.01	2.76
Xuchang	6.89	2.83	6.19	2.18	6.67	2.36
Luohe	7.60	2.66	6.99	2.40	7.20	2.46
Sanmenxia	4.76	2.16	4.75	1.78	4.85	1.84
Nanyang	5.03	1.67	4.71	2.18	4.93	1.85
Shangqiu	6.38	2.56	5.25	2.81	6.04	2.61
Xinyang	6.14	1.17	5.68	1.55	5.91	1.95
Zhoukou	6.45	2.42	6.29	2.12	6.38	2.17
Zhumadian	5.79	1.90	5.73	2.13	5.91	2.12
Jiyuan	5.38	2.78	4.75	2.22	5.15	2.26

* Mean yield from 2018 to 2020.

Table 7. Annual crop planted areas of various cities in Henan Province, China.

Cities	Mean Planted Areas * (kha)		Planted Areas in 2021 (kha)		Planted Areas in 2022 (kha)	
	Corn	Beans	Corn	Beans	Corn	Beans
Zhengzhou	134.57	6.26	127.87	4.22	127.64	4.85
Kaifeng	189.32	13.19	187.67	12.00	186.41	14.28
Luoyang	182.16	29.95	196.55	19.90	194.40	23.48
Pingdingshan	198.00	14.09	197.36	13.82	196.73	15.29
Anyang	247.33	4.76	251.56	4.01	253.29	6.30
Hebi	77.90	0.52	78.21	0.37	77.76	1.68
Xinyang	293.59	14.80	309.27	9.62	310.12	12.63
Jiaozuo	121.33	4.41	126.39	1.97	126.96	3.08
Puyang	145.86	23.72	153.27	22.74	155.33	24.70
Xuchang	151.04	42.97	153.59	41.57	155.24	42.03
Luohe	85.68	34.13	92.88	29.58	93.40	30.53
Sanmenxia	58.01	20.95	60.27	19.39	60.20	19.52
Nanyang	454.36	49.97	467.86	33.74	470.35	37.48
Shangqiu	429.03	52.23	445.71	35.74	439.51	42.86
Xinyang	20.99	7.15	15.62	4.40	18.90	3.13
Zhoukou	511.48	104.54	542.82	75.76	544.11	76.67
Zhumadian	435.87	26.19	438.83	25.07	434.85	30.59
Jiyuan	19.91	1.32	20.05	1.34	20.53	1.32

* Mean planted areas from 2018 to 2020.

4.4. Limitations and Outlook

The second-growing season crops in Henan have been boosted by subsidy policies in recent years, so their plantings are increasing annually. According to the 2023 Statistical Yearbook released by the Henan Provincial People's Government, the area of fall crops in the province expanded by 17.84 kha in 2022. This shift not only affected local agricultural yield but also contributed to advancing the SOS to a certain extent. This trend of varietal

switching and altered planting density introduces a slew of new challenges and opportunities for both ecological environment and climate response patterns in Henan, which deserves further in-depth study and exploration. The data covered in this study were limited to 3 years after the extreme rainfall event occurred, and the yield data for 2023 are not yet available online and so could not be analyzed in conjunction with other factors, such as sunshine hours and wind speed. Moreover, the effect of soil moisture on NDVI values may be significant at local scales, especially in sparsely vegetated areas, where wetter soils may lead to higher reflectance. It should be noted that this paper is based on statistical analyses performed on a whole-province scale, which did not specifically consider soil moisture effects. Hence, a comprehensive understanding of vegetation restoration dynamics requires continued observation and research over the long term. Future research activity could consider a wider range of environmental variables, including factors such as soil moisture, wind speed, temperature fluctuations, and human intervention, to better understand the long-term effects of extreme rainfall events on vegetation phenology.

5. Conclusions

This unique case study provides insight into differential phenology responses to an extreme rainfall event among vegetation types in Henan Province, China. Vegetation phenology in Henan was extracted from MODIS reflectance data from 2018 to 2023. Significant differences between SOS and EOS after and before the event were analyzed, along with the resistance and recovery of vegetation, the recovery rate of rainfall, the factors affecting NDVI, and the relationships of rainfall to phenological indicators and crop yield. The main conclusions are as follows:

(1) The application of Duncan's analysis was crucial in detecting significant differences between treatment groups after extreme rainfall events, providing robust statistical support for the results. The effect of an extreme rainfall event on phenology directly manifested as a delay in the EOS of the year of the event. In 2021, the EOS of the second growing season was delayed by 4.97 days for cropland, 15.54 days for forest, 13.06 days for grassland, and 12.49 days for shrubland.
(2) Resistance decreased in forest, grassland, and shrubland after the extreme rainfall event. Recovery was good in most areas 1 year after the event, and phenology parameters did not recover 2 years after the event.
(3) The extreme rainfall event negatively impacted crop yields in autumn 2021, and the correlation between yield and rainfall was negative in most areas. The study underscores the need for effective disaster management strategies in agricultural regions prone to extreme weather, particularly in economically vital areas like Henan Province.

There is a clear correlation between phenology and rainfall, which is generally expressed as a negative correlation between SOS and rainfall of the first growing season in cropland, grassland, and shrubland, but as a positive correlation between EOS and rainfall of the first and second growing seasons in cropland and shrubland. The results of this study suggest that attention should be paid to the significant losses caused by extreme rainfall to society and to finding ways to minimize the impact of associated flooding. The government of Henan, given its status as a nationally important economic and grain-producing province, should aim to strengthen disaster prevention and improve urban planning to lessen the potential impact of future extreme weather events on its society and economy.

Author Contributions: Conceptualization, Y.L. (Yinghao Lin), Q.G. and Y.W. (Yuye Wang); methodology, Y.L. (Yinghao Lin), Q.G. and Y.W. (Yuye Wang); software, X.G.; validation, Q.G., Y.L. (Yang Liu) and Y.W. (Yadi Wang); formal analysis, L.Z.; investigation, X.G.; resources, Y.L. (Yinghao Lin); data curation, Y.L. (Yinghao Lin) and X.G.; writing—original draft preparation, X.G.; writing—review and editing, Y.L. (Yinghao Lin) and Q.G.; visualization, Y.W. (Yadi Wang); supervision, Q.G.; project administration, Q.G.; funding acquisition, Y.L. (Yinghao Lin). All authors have read and agreed to the published version of the manuscript.

Funding: This research was funded by the Science and Technology Development Program of Henan Province (No. 242300421639); the Shenzhen Science and Technology Program (No. JCYJ20220530162001003); the Key R&D and Promotion Projects of Henan Province (No. 232102210071); the National Science and Technology Major Project (No. 80-Y50G19-9001-22/23); and a Scientific and Technological Innovation Team of Universities in Henan Province (No. 24IRTSTHN021).

Institutional Review Board Statement: Not applicable.

Data Availability Statement: The dataset used in this paper can be found through the National Basic Geographic Information Center of China: https://www.ngcc.cn/ (accessed on 10 March 2024), the National Oceanic and Atmospheric Administration: https://www.ncei.noaa.gov/ (accessed on 29 March 2024), the Google Earth Engine: https://code.earthengine.google.com/ (accessed on 15 April 2024), and the Henan Provincial Bureau of Statistics: https://tjj.henan.gov.cn/tjfw/tjcbw/tjnj/ (accessed on 15 May 2024).

Acknowledgments: The author would like to thank all contributors to this study.

Conflicts of Interest: The authors declare no conflicts of interest.

References

1. Barichivich, J.; Briffa, K.R.; Osborn, T.J.; Melvin, T.M.; Caesar, J. Thermal growing season and timing of biospheric carbon uptake across the Northern Hemisphere. *Glob. Biogeochem. Cycles* **2012**, *26*, GB4015. [CrossRef]
2. Badeck, F.W.; Bondeau, A.; Böttcher, K.; Doktor, D.; Lucht, W.; Schaber, J.; Sitch, S. Responses of spring phenology to climate change. *New Phytol.* **2004**, *162*, 295–309. [CrossRef]
3. Zhang, J.; Chen, S.; Wu, Z.; Fu, Y. Review of vegetation phenology trends in China in a changing climate. *Prog. Phys. Geogr.* **2022**, *46*, 829–845. [CrossRef]
4. Shen, M.; Piao, S.; Cong, N.; Zhang, G.; Jassens, I.A. Precipitation impacts on vegetation spring phenology on the Tibetan Plateau. *Glob. Chang. Biol.* **2015**, *21*, 3647–3656. [CrossRef] [PubMed]
5. Piao, S.; Zhang, X.; Chen, A.; Liu, Q.; Lian, X.; Wang, X.; Peng, S.; Wu, X. The impacts of climate extremes on the terrestrial carbon cycle: A review. *Sci. China Earth Sci.* **2019**, *62*, 1551–1563. [CrossRef]
6. Gong, Y.; Staudhammer, C.L.; Kenney, G.; Wiesner, S.; Zhang, Y.; Starr, G. Vegetation structure drives forest phenological recovery after hurricane. *Sci. Total Environ.* **2021**, *774*. [CrossRef]
7. Liu, Q.; Fu, Y.H.; Zeng, Z.; Huang, M.; Li, X.; Piao, S. Temperature, precipitation, and insolation effects on autumn vegetation phenology in temperate China. *Glob. Chang. Biol.* **2016**, *22*, 644–655. [CrossRef]
8. Sun, M.; Li, P.; Ren, P.; Tang, J.; Zhang, C.; Zhou, X.; Peng, C. Divergent response of vegetation phenology to extreme temperatures and precipitation of different intensities on the Tibetan Plateau. *Sci. China Earth Sci.* **2023**, *66*, 2200–2210. [CrossRef]
9. Zhang, N.; Qu, Y.; Song, Z.; Chen, Y.; Jiang, J. Responses and sensitivities of maize phenology to climate change from 1971 to 2020 in Henan Province, China. *PLoS ONE* **2022**, *17*, e0262289. [CrossRef]
10. Liu, Y.; Qin, Y.; Ge, Q.; Dai, J.; Chen, Q. Reponses and sensitivities of maize phenology to climate change from 1981 to 2009 in Henan Province, China. *J. Geogr. Sci.* **2017**, *27*, 1072–1084. [CrossRef]
11. He, Z.; Du, J.; Chen, L.; Zhu, X.; Lin, P.; Zhao, M.; Fang, S. Impacts of recent climate extremes on spring phenology in arid-mountain ecosystems in China. *Agric. For. Meteorol.* **2018**, *260–261*, 31–40. [CrossRef]
12. Zhang, Q.; Li, R.; Sun, J.; Lu, F.; Xu, J.; Zhang, F. A Review of Research on the Record-Breaking Precipitation Event in Henan Province, China, July 2021. *Adv. Atmos. Sci.* **2023**, *40*, 1485–1500. [CrossRef]
13. Lan, Q.; Dong, J.; Lai, S.; Wang, N.; Zhang, L.; Liao, M. Flood Inundation Extraction and its Impact on Ground Subsidence Using Sentinel-1 Data: A Case Study of the "7.20" Rainstorm Event in Henan Province, China. *IEEE J. Sel. Top. Appl. Earth Obs. Remote Sens.* **2024**, *17*, 2927–2938. [CrossRef]
14. Rahman, M.S.; Di, L. A Systematic Review on Case Studies of Remote-Sensing-Based Flood Crop Loss Assessment. *Agriculture* **2020**, *10*, 131. [CrossRef]
15. Himani Kanwar, S.S. Phenology and Global Climate Change: A Comprehensive Review. *eJournal Appl. For. Ecol. (eJAFE)* **2023**, *11*, 20–30.
16. Pan, L.; Xia, H.; Zhao, X.; Guo, Y.; Qin, Y. Mapping Winter Crops Using a Phenology Algorithm, Time-Series Sentinel-2 and Landsat-7/8 Images, and Google Earth Engine. *Remote Sens.* **2021**, *13*, 2510. [CrossRef]
17. Shi, B.; Zhu, X.; Hu, Y.; Yang, Y. Drought characteristics of Henan province in 1961-2013 based on Standardized Precipitation Evapotranspiration Index. *J. Geogr. Sci.* **2017**, *27*, 311–325. [CrossRef]
18. Huang, J.; Zhou, L.; Zhang, F.; Hu, Z.; Tian, H. Responses of yield variability of summer maize in Henan province, north China, to large-scale atmospheric circulation anomalies. *Theor. Appl. Climatol.* **2021**, *143*, 1655–1665. [CrossRef]
19. The People's Government of Henan Province. Provincial Situation. Available online: https://www.henan.gov.cn/2024/08-08/3033664.html (accessed on 26 August 2024).
20. Kong, D.; McVicar, T.R.; Xiao, M.; Zhang, Y.; Peña-Arancibia, J.L.; Filippa, G.; Xie, Y.; Gu, X. phenofit: An R package for extracting vegetation phenology from time series remote sensing. *Methods Ecol. Evol.* **2022**, *13*, 1508–1527. [CrossRef]

21. NGCC. National Geomatics Center of China. Available online: https://www.ngcc.cn/ (accessed on 10 March 2024).
22. Testa, S.; Soudani, K.; Boschetti, L.; Borgogno Mondino, E. MODIS-derived EVI, NDVI and WDRVI time series to estimate phenological metrics in French deciduous forests. *Int. J. Appl. Earth Obs. Geoinf.* **2018**, *64*, 132–144. [CrossRef]
23. Zeng, L.; Wardlow, B.D.; Hu, S.; Zhang, X.; Zhou, G.; Peng, G.; Xiang, D.; Wang, R.; Meng, R.; Wu, W. A Novel Strategy to Reconstruct NDVI Time-Series with High Temporal Resolution from MODIS Multi-Temporal Composite Products. *Remote Sens.* **2021**, *13*, 1397. [CrossRef]
24. Liu, W. The Response of NDVI to Drought at Different Temporal Scales in the Yellow River Basin from 2003 to 2020. *Water* **2024**, 16. [CrossRef]
25. Gorelick, N.; Hancher, M.; Dixon, M.; Ilyushchenko, S.; Thau, D.; Moore, R. Google Earth Engine: Planetary-scale geospatial analysis for everyone. *Remote Sens. Environ.* **2017**, *202*, 18–27. [CrossRef]
26. Vermote, E.; Wolfe, R. MODIS/Terra Surface Reflectance Daily L2G Global 1 km and 500 m SIN Grid V061. 2021. Available online: https://lpdaac.usgs.gov/products/mod09gav061/ (accessed on 15 April 2024).
27. Joshi, R.; Singh, A.; Parab, T.; Mandy, J.; Pande, C. Assessing the Impact of Recent Climate Dynamics on Land Since the Last Two Decades (1991–2021) Using LST and NDVI. In *Natural Resource Monitoring, Planning and Management Based on Advanced Programming*; Advances in Geographical and Environmental Sciences; Springer: Singapore, 2024; pp. 269–308.
28. Rocha, A.V.; Shaver, G.R. Advantages of a two band EVI calculated from solar and photosynthetically active radiation fluxes. *Agric. For. Meteorol.* **2009**, *149*, 1560–1563. [CrossRef]
29. Jiang, Z.; Huete, A.; Didan, K.; Miura, T. Development of a two-band enhanced vegetation index without a blue band. *Remote Sens. Environ.* **2008**, *112*, 3833–3845. [CrossRef]
30. Statistical Yearbook of Henan Provincial Bureau of Statistics. Available online: https://tjj.henan.gov.cn/tjfw/tjcbw/tjnj/ (accessed on 15 May 2024).
31. Xie, P.; Robert, J.; Wu, S.; Yoo, S.-H.; Yarosh, Y.; Sun, F.; Lin, R. NOAA CDR Program. NOAA Climate Data Record (CDR) of CPC Morphing Technique (CMORPH) High Resolution Global Precipitation Estimates, Version 1. 2019. 2024. Available online: https://www.ncei.noaa.gov/access/metadata/landing-page/bin/iso?id=gov.noaa.ncdc:C00948 (accessed on 29 March 2024).
32. R Core Team. *R: A Language and Environment for Statistical Computing*; R Foundation for Statistical Computing: Vienna, Austria, 2024; Available online: https://www.R-project.org/ (accessed on 11 May 2024).
33. Kim, S.; Ouyang, M.; Zhang, X. Compute spearman correlation coefficient with Matlab/CUDA. In Proceedings of the 2012 IEEE International Symposium on Signal Processing and Information Technology (ISSPIT), Ho Chi Minh City, Vietnam, 12–15 December 2012; pp. 000055–000060.
34. Rodrigues, L.; Paixao, E. Risk of Zika-related microcephaly: Stable or variable? *Lancet* **2017**, *390*, 824–826. [CrossRef]
35. Portela, A.P.; Goncalves, J.F.; Durance, I.; Vieira, C.; Honrado, J. Riparian forest response to extreme drought is influenced by climatic context and canopy structure. *Sci. Total Environ.* **2023**, *881*, 163128. [CrossRef]
36. Lin, C.-Y.; Lo, H.-M.; Chou, W.-C.; Lin, W.-T. Vegetation recovery assessment at the Jou-Jou Mountain landslide area caused by the 921 Earthquake in Central Taiwan. *Ecol. Model.* **2004**, *176*, 75–81. [CrossRef]
37. Hong, Y.; Zhao, Y.; Wang, Y.; Xin, C.; Zhao, Y. Temporal and spatial variation characteristics of vegetation restoration based on MODIS-NDVI Wenchuan earth quake region in ten years. *Sci. Tecnol. Eng.* **2019**, *19*, 64–71.
38. Li, M.; Li, G.; Xie, Z. Post-flood recovery assessment based on multi-source remote sensing data: A case study of the "7·20" rainstorm in Henan. *Remote Sens. Nat. Resour.* **2024**, *36*, 250–266. [CrossRef]
39. Ying, H.; Zhang, H.; Zhao, J.; Shan, Y.; Zhang, Z.; Guo, X.; Rihan, W.; Deng, G. Effects of spring and summer extreme climate events on the autumn phenology of different vegetation types of Inner Mongolia, China, from 1982 to 2015. *Ecol. Indic.* **2020**, *111*, 105974. [CrossRef]
40. Karimi, S.; Heydari, M.; Mirzaei, J.; Karami, O.; Heung, B.; Mosavi, A. Assessment of Post-Fire Phenological Changes Using MODIS-Derived Vegetative Indices in the Semiarid Oak Forests. *Forests* **2023**, *14*, 590. [CrossRef]
41. Weaver, B.; Wuensch, K.L. SPSS and SAS programs for comparing Pearson correlations and OLS regression coefficients. *Behav. Res. Methods* **2013**, *45*, 880–895. [CrossRef]
42. Elephant Entertainment. How Heavy Is the Rainfall in Henan during This Year's Flood Season? Rainfall in Multiple Areas Breaks Historical Records. Available online: https://baijiahao.baidu.com/s?id=1673085675293448809&wfr=spider&for=pc (accessed on 2 April 2024).
43. Henan Hydrological and Water Resources Monitoring and Reporting Center. Monthly Water Situation Report for July 2022. Available online: http://www.hnssw.com.cn/sqwater1/31705.jhtml (accessed on 3 April 2024).
44. Henan Hydrological and Water Resources Monitoring and Reporting Center. Monthly Water Situation Report for July 2023. Available online: http://www.hnssw.com.cn/l1SwfwL2Sqxx/34398.jhtml (accessed on 5 April 2024).
45. Hogan, J.A.; Feagin, R.A.; Starr, G.; Ross, M.; Lin, T.-C.; O'connell, C.; Huff, T.P.; Stauffer, B.A.; Robinson, K.L.; Lara, M.C.; et al. A Research Framework to Integrate Cross-Ecosystem Responses to Tropical Cyclones. *BioScience* **2020**, *70*, 477–489. [CrossRef]
46. LI, R.; Zhou, G. Responses of woody plants phenology to air temperature in Northeast China in 1980–2005. *Chin. J. Ecol.* **2010**, *29*, 2317–2326. [CrossRef]
47. Piao, S.; Fang, J.; Zhou, L.; Ciais, P.; Zhu, B. Variations in satellite-derived phenology in China's temperate vegetation. *Glob. Chang. Biol.* **2006**, *12*, 672–685. [CrossRef]

48. Jeong, S.-J.; Ho, C.-H.; Gim, H.-J.; Brown, M.E. Phenology shifts at start vs. end of growing season in temperate vegetation over the Northern Hemisphere for the period 1982–2008. *Glob. Chang. Biol.* **2011**, *17*, 2385–2399. [CrossRef]
49. Hwang, T.; Song, C.; Vose, J.M.; Band, L.E. Topography-mediated controls on local vegetation phenology estimated from MODIS vegetation index. *Landsc. Ecol.* **2011**, *26*, 541–556. [CrossRef]
50. Renton, K.; Salinas-Melgoza, A.; Rueda-Hernández, R.; Vázquez-Reyes, L.D. Differential resilience to extreme climate events of tree phenology and cavity resources in tropical dry forest: Cascading effects on a threatened species. *Forest Ecol.* **2018**, *426*, 164–175. [CrossRef]
51. Hu, X.; Huang, B.; Cherubini, F. Impacts of idealized land cover changes on climate extremes in Europe. *Ecol. Indic.* **2019**, *104*, 626–635. [CrossRef]
52. Li, C.; Wang, J.; Hu, R.; Yin, S.; Bao, Y.; Ayal, D.Y. Relationship between vegetation change and extreme climate indices on the Inner Mongolia Plateau, China, from 1982 to 2013. *Ecol. Indic.* **2018**, *89*, 101–109. [CrossRef]
53. Huang, Y.; Chen, X.S.; Zou, Y.A.; Zhang, P.Y.; Li, F.; Hou, Z.Y.; Li, X.; Zeng, J.; Deng, Z.M.; Zhong, J.R.; et al. Exploring the relative contribution of flood regimes and climatic factors to Carex phenology in a Yangtze River-connected floodplain wetland. *Sci. Total Environ.* **2022**, *847*, 157568. [CrossRef] [PubMed]
54. Zhang, X.; Friedl, M.A.; Schaaf, C.B.; Strahler, A.H.; Liu, Z. Monitoring the response of vegetation phenology to precipitation in Africa by coupling MODIS and TRMM instruments. *J. Geophys. Res. Atmos.* **2005**, *110*, 1–14. [CrossRef]
55. Zscheischler, J.; Michalak, A.M.; Schwalm, C.; Mahecha, M.D.; Huntzinger, D.N.; Reichstein, M.; Berthier, G.; Ciais, P.; Cook, R.B.; El-Masri, B.; et al. Impact of large-scale climate extremes on biospheric carbon fluxes: An intercomparison based on MsTMIP data. *Glob. Biogeochem. Cycles* **2014**, *28*, 585–600. [CrossRef]
56. Liu, Y.; Shi, W. The quantitative impacts of drought and flood on crop yields and production in China. In Proceedings of the 2019 8th International Conference on Agro-Geoinformatics (Agro-Geoinformatics), Istanbul, Turkey, 16–19 July 2019; pp. 1–6.
57. Pantaleoni, E.; Engel, B.A.; Johannsen, C.J. Identifying agricultural flood damage using Landsat imagery. *Precis. Agric.* **2007**, *8*, 27–36. [CrossRef]